Bottom-Up Approach to Innovative Memory Devices: I. Intrinsic and Environmental Effects on the Molecular Component

Ilaria Pino, Luca Sementa, Mauro Causà, and Vincenzo Barone*,†,‡,§

Dipartimento di Chimica, Universitá degli Studi "Federico II", Complesso Monte S. Angelo, Via Cintia, I-80126 Napoli, Italy

Received: May 14, 2008; Revised Manuscript Received: August 5, 2008

The 50 nm-thick polystyrene (PS) film, involved in some innovative memory devices, contains 8-hydroxyquinoline (8HQ) molecules and gold nanoparticles. A model where molecular localized properties directly reflect on macroscopic behavior of a complex system has been tested in the present work, which is focused on the structural and electronic properties of the 8HQ-PS mixture modeled in a continuum scheme: one 8HQ molecule with a polarizable continuum model (PCM) whose reliability has been checked by comparison with periodic DFT calculations of 8HQ-PS crystalline structures. A comprehensive study of the keto−enolic tautomerization of 8HQ has been performed, at the DFT level using B3LYP, LC-PBE, and M052X functionals and a polarized double-ζ basis set. The energetics of the obtained structures (minima and transition states) have been refined by single point calculations at the CCSD(T) level with the aug-cc-pVDZ basis set. Our calculations predict the enolic tautomer to be the most stable for the isolated and PS-solvated 8HQ in its neutral form, with a tautomerization barrier much larger than the thermal energy at the working conditions. The opposite trend has been found for the charged (both positive and negative) 8HQ, with ketonic tautomers being the most stable. In a first approximation of weak interaction with the aluminum electrodes, the electric-field effects have also been taken into account for the calculations of electron affinities and ionization potentials of 8HQ molecules. The electron and hole injection barriers issuing from these results are in good agreement with the experimental observations.

1. Introduction

Bistable organic electronic devices are very promising for applications in several fields of current technological interest, like nonvolatile computer memories.[1−5] Yang and co-workers describe an organic memory device, constituted by a sandwich of a solid solution of 8-hydroxyquinoline (8HQ) in polystyrene (PS), between condenserlike aluminum electrodes.[6] In the polystyrene/8-hydroxyquinoline matrix, gold nanoparticles (AuNP) are diluted, after surface functionalization, with 1-dodecanethiols. The most interesting characteristics of this class of devices is the amazing simplicity of their structure, and so, the economic advantage in their production with respect to conventional semiconductor-based memory devices, that are composed by many layers of different materials. It is also important to take into account the environmental advantages of organic electronic components, in term of their lower energy content and of the less hazardous chemicals involved in their preparation.

A deeper understanding of the key physicochemical factors tuning the behavior of organic electronic devices is a mandatory prerequisite for optimizing the structure and the composition of the materials, for approaching the performances, the stability, and the reliability of the corresponding semiconductor devices, or even for projecting new components.[7] The present study represents the first step of a project aimed at understanding the various aspects of the Yang's organic memory device, using the tools of computational chemistry. In spite of the apparent simplicity of this device, the accurate description of electric phenomena at the atomic level is a very difficult task, because it involves many problems that are at the frontier of the theoretical chemistry and solid state physics. In this work, a molecular level approach has been tested, where the single component identities remain basically unaffected by interactions and their properties directly reflect on the macroscopic properties.

The Yang's organic memory device is composed by the following subsystems: the interface between the aluminum electrodes and the PS−8HQ mixture itself; the interface between the AuNP and the PS−8HQ mixture. In the present paper, the structural and electronic properties of the PS−8HQ mixture will be taken into account: our first aim is to describe the low-conductivity regime of the device throwing light on the thermodynamics to be obeyed for electronic switching to the high-conductivity state. The latter aim is achieved by accurately calculating the electron affinities (EA) and ionization potentials (IP) of the 8HQ molecules in this specific environment. In fact, the EAs and IPs are necessary to obtain the electron and hole injection barriers at the metals−organic matrix interfaces, which represent the energies to be overcome for the electron transfer between the metals and the 8HQ molecules.[8−10]

The present work is organized as follows. The second section provides a brief account of the computational methods and theoretical models. The third section shows the results of the keto−enolic tautomerization of the differently charged 8HQ in vacuum as obtained at different levels of theory to strike a balance between accuracy and feasibility in quantum mechanical (QM) calculations for the description of both thermodynamics and kinetics properties of this system. In the fourth section, the

* To whom correspondence should be addressed. E-mail: baronev@unina.it.
† IPCF-CNR, Area della Ricerca, via G. Moruzzi 1, I-56124 Pisa, Italy.
‡ INFN−Sezione di Perugia, via A. Pascoli, 06123 Perugia, Italy.
§ IMAST P.le Enrico Fermi 1, Localita Granatello Portici, I-80055 Napoli, Italy.

10.1021/jp804274r CCC: $40.75
Published on Web 10/15/2008

polystyrene role is investigated by comparing its explicit interaction with 8HQ and its solely polarization and solvation effects on 8HQ. In the fifth section, we study the effect of applied electric fields to the system and we show the estimated electron and hole injection barriers at the interfaces of gold nanoparticles−8HQ/PS and aluminum−8HQ/PS. A summary of results and conclusions are presented in the sixth section.

2. Computational Methods

We have performed molecular DFT (closed- and open-shell) calculations with a local version of the Gaussian suite of programs for quantum chemistry.[11] We exploited the well-known B3LYP exchange-correlation functional[12] and the recently developed M052X[13,14] and LC-PBE-TPSS[15] functionals, which should better account for medium−long-range interactions. We adopted the polarizable continuum model (PCM) for molecule−solvent interactions[16−20] with Pauling radii definitions, and we considered the contribution of homogeneous electric fields along a direction in the determination of 8HQ structures and electronic properties.[21] A locally optimized basis set of polarized double-ζ level (N07D) has been used for all non periodic DFT molecular calculations.[22] Optimizations of transition states and minimum energy reaction paths were obtained according to the QST3 ansatz.[23]

Molecular coupled cluster (closed- and open-shell) calculations[24,25] were performed by the MOLPRO package[26] with the aug-cc-pVDZ basis set.[27]

The molecular mechanics structure optimizations have been performed with the Discover module of the Materials Studio 4.0 program,[28] using the CVFF force field.[29−31] Figure 2 is also made using Materials Studio.

Periodic DFT calculations were performed on bulk crystals with the CRYSTAL06 program.[32,33] The periodicity was considered by using the space symmetry; the infinite series of Coulombic integrals was approximated with Ewald techniques,[34] whereas the infinite exchange series, representing an essentially short-range interaction, was truncated to ensure convergence for energy and related observables.[35] The solution of the effective one-electron Schrödinger equation was performed in reciprocal space. The *k* points (2, 2) were sampled on a regular mesh.[36] The symmetry was fully implemented in direct space, to minimize the number of molecular integrals that needed to be computed and stored, and in reciprocal space, to perform a block diagonalization.[37] Energy derivatives with respect to the position of the atoms in the unit cell were recently implemented,[38−40] thus making it possible to optimize the equilibrium geometry within a given crystal symmetry automatically. The B3LYP hybrid density functional[12] was used at the all-electron level using 6-31G* Gaussian atomic orbitals, corresponding to a polarized double-ζ basis set.[41]

3. 8HQ Structures and Energetics

The 8HQ is a largely studied molecule, in solid state and in solution, both experimentally[42−45] and theoretically.[45−47] Also known with the name of oxin, 8HQ is the second most important chelating agent used in analytical chemistry for detecting and quantifying metals in solution. Its bifunctional structure permits the formation of intramolecular and intermolecular hydrogen bonds, and it can undergo keto−enolic tautomerization, the extent depending on the solvent (see Figure 1).

Diffraction data of solid 8HQ reveals an intermolecularly H-bonded dimeric structure, but they are not able to establish the monomer tautomeric form.[43,44] Indeed, a theoretical study shows evidence of how keto-monomers form the most stable

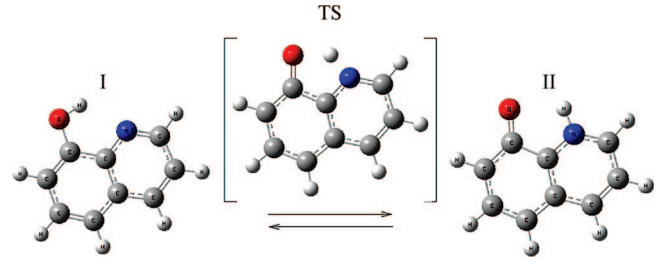

Figure 1. Enolic (I) and ketonic (II) tautomers of 8HQ.

H-bonded dimers.[47] However, the low melting point along with the infrared spectra information of pure 8HQ seem to suggest the more likely occurrence of intramolecular H-bonds against the intermolecular ones.[45] In water, the tautomerization of 8HQ would occur via a competition between intermolecular and intramolecular proton transfers, whereas in alkane solvents 8HQ dimers are observed which undergo concerted biprotonic transfers.[45] Hydrated forms also exist in chlorinated solvents, in benzene and in toluene, and infrared spectra of diluted 8HQ in CCl_4 reveal the exclusive presence of the enolic form.[42,45] However, the quantity of 8HQ in the anhydrous environment of the memory device is too small for the occurrence of relevant intermolecular interactions and the existence of a regular dimeric structure is unlikely. Indeed 8HQ molecules are at a mean distance of 6−10 Å from each other.[6] To determine which tautomeric form is the most stable in the device environment, we first performed geometrical optimizations of the isolated 8HQ by means of DFT theory with three different functionals, B3LYP, LC-PBE-TPSS, and M052X. Equilibrium structures and transition states are required to state the tautomerization rate. As is well-known from literature, the reaction barriers may be underestimated by DFT calculations,[14] which are, instead, able to predict accurate equilibrium geometrical structures. To refine energies, we then calculated single-point energies of molecular DFT-optimized structures at a more accurate level of theory, namely the coupled cluster method CCSD(T) with single, double, and perturbative triple excitations, which is the method of choice for reference purposes when multireference effects are negligible. Indeed, we are interested in determining not only the relative thermodynamical stability of the different tautomers but also the energy barriers between them in order to estimate the relative quantities of the two tautomeric species and the rates of interconversion at nanoscale times. In Table 1, we show in the first column the total energy of the enolic (I) tautomers for the neutral, negative, and positive 8HQ at different levels of theory: DFT calculations are compared with the CCSD(T) energies calculated with the B3LYP-optimized geometries. It is worth noting that the CCSD(T) energies calculated with LC-PBE-TPSS and M052X optimized structures are slightly higher than those reported in Table 1. So, in this context, we can conclude that the B3LYP functional provides the best geometries. At any level of theory here adopted, the enolic form results in being the most stable (by 0.8 eV) when 8HQ is neutral, whereas the ketonic form is preferred for charged 8HQ molecules with an energy difference of 0.01 and 0.3 eV for the negative and positive 8HQ, respectively. It can be noted from results in Table 1 that, among the three different DFT functionals, the LC-PBE-TPSS total energies show the best agreement with CCSD(T) values. However, rather than total energies we are interested in energy differences which provide relative stabilities between tautomers, tautomerization barriers, ionization potentials (IPs), and electron affinities (EAs). In Table 1, we also show the comparison between DFT and CCSD(T) calculations of the energy differences between enolic and ketonic

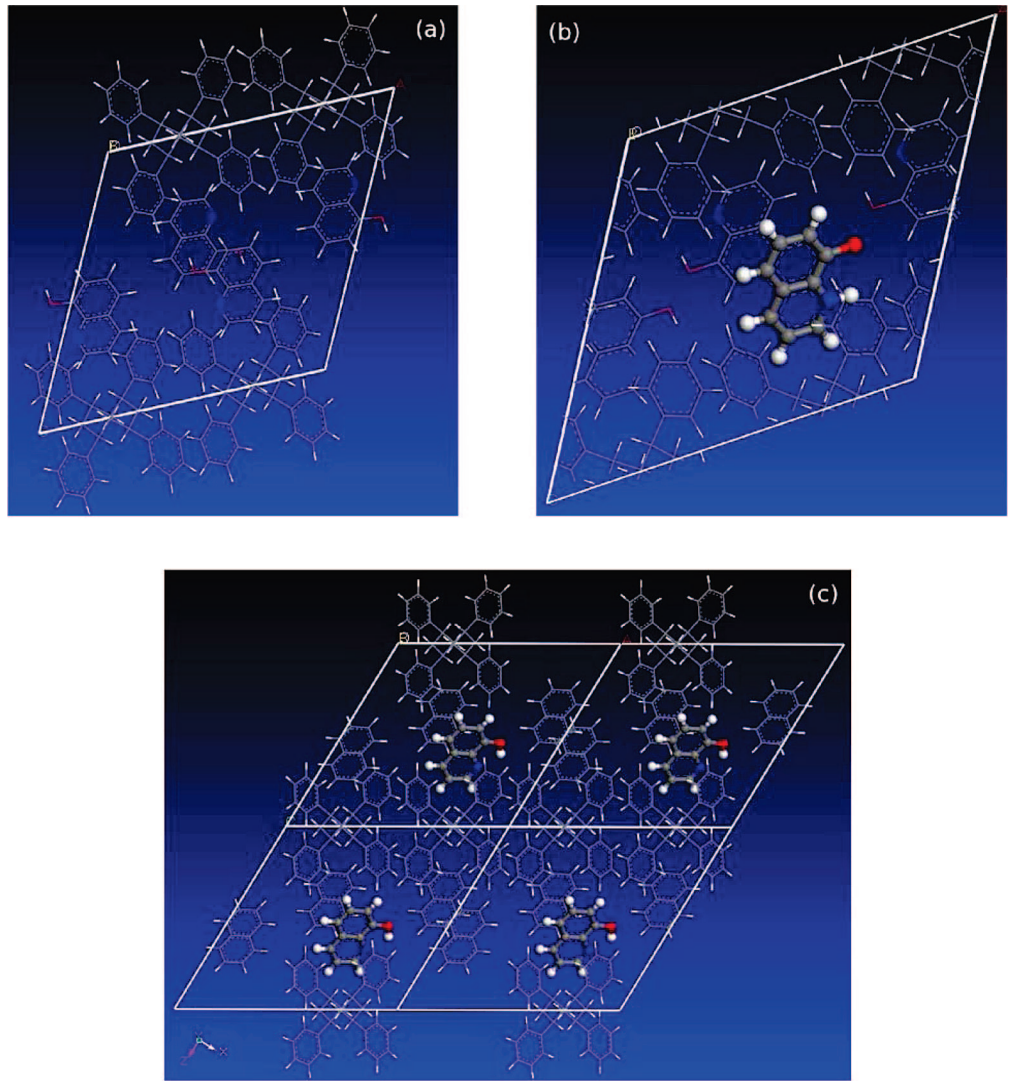

Figure 2. Crystalline models of s-PS intercalates with 8HQ moieties. The [010] axis is perpendicular to the picture: (a) 8HQ molecules are enolic, and the crystal is in the $P2_1/a$ space group. (b) 8HQ molecules are enolic except one in the ketonic form, and the crystal is in the $P1$ space group. (c) The [100] axis is directed to the right-hand. One 8HQ with three naphthalene molecules in the unit cell.

TABLE 1: Comparison between DFT (B3LYP, LC-PBE-TPSS, and M052X) and CCSD(T) Calculations of Neutral, Negative, and Positive 8HQ: Total Energy E_I of the Enolic Tautomers, Relative Stability of Enolic (I) and Ketonic (II) Forms ($E_I - E_{II}$), and Tautomerization Barriers[a]

method	charge	E_I	$E_I - E_{II}$	$\Delta E^{\ddagger}_{I\to II}$	$\Delta E^{\ddagger}_{II\to I}$
B3LYP	0	−477.198162	−63.4	84.5	21.0
LC-PBE-TPSS	0	−475.630095	−78.0	82.2	4.2
M052X	0	−477.147699	−78.1	91.6	13.5
CCSD(T)	0	−475.955680	−78.0	94.2	16.2
B3LYP	−1	−477.207211	7.6	43.8	51.4
LC-PBE-TPSS	−1	−475.644033	7.3	29.1	36.5
M052X	−1	−477.154439	1.8	43.4	45.1
CCSD(T)	−1	−475.959461	1.3	46.9	48.2
B3LYP	1	−476.913444	28.0	43.0	71.0
LC-PBE-TPSS	1	−475.334574	30.3	25.8	56.0
M052X	1	−476.857323	23.1	43.0	66.1
CCSD(T)	1	−475.667246	30.8	41.2	72.0

[a] E_I is expressed in Hartree whereas energy differences are in kilojoules per mole.

tautomers and of both tautomerization barriers. We further show the ionization potentials and electron affinities in Table 2 as resulting from considering the enolic form for the neutral 8HQ and the keto forms for the charged molecules. The M052X functional turns out to globally give the most reasonable DFT results both for relative stability of tautomers and tautomerization barriers. The better accuracy of M052X is much more evident in prediction of small energy differences as in the case of relative stability of the negative tautomers: the relative error on this energy improves from 464% to 28% by using B3LYP and M052X, respectively. However, a reasonable agreement between B3LYP and CCSD(T) ionization potentials is found. In conclusion, from a general trend, we decided to adopt the M052X functional for further DFT molecular calculations where the PS matrix and electric field effects will be taken into account to some extent.

TABLE 2: Electron Affinities and Ionization Potentials As Resulting from the Energy Differences $E_I - E_{II}^-$ and $E_{II}^+ - E_I$, Respectively[a]

method	EA_{vac}	IP_{vac}
B3LYP	0.33	7.46
LC-PBE-TPSS	0.46	7.73
M052X	0.20	7.66
CCSD(T)	0.12	7.53

[a] Energies are in electonvolts.

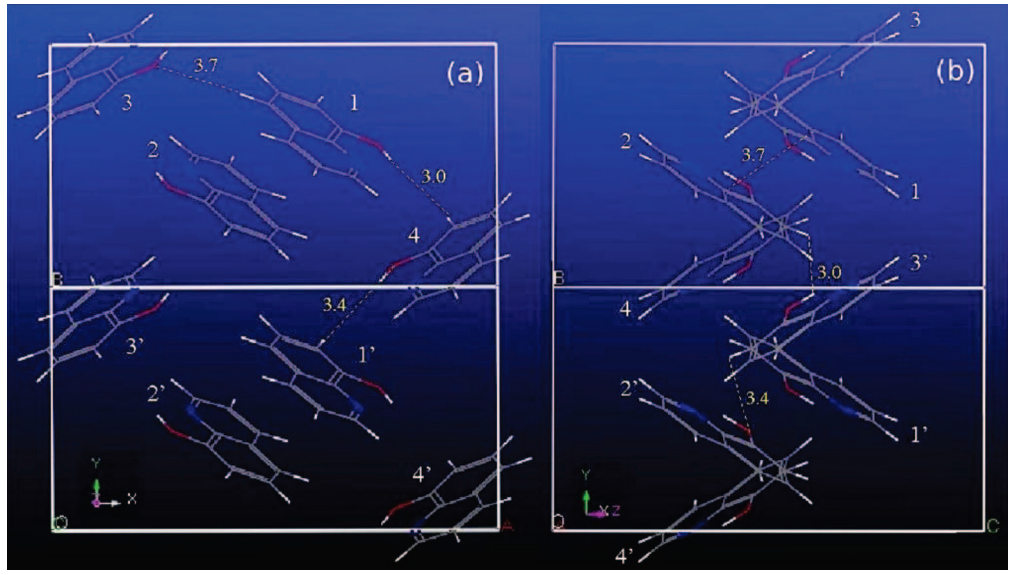

Figure 3. 8HQ sublattice in the unit cell of the s-PS intercalate. Some internuclear distances of adjacent molecules have been shown in angstroms (yellow numbers and dashed lines). 8HQ molecules have been labeled with numbers and numbers prime to highlight the equivalence for translational symmetry. (a) (001) plane projection; (b) (100) plane projection.

4. 8HQ/PS Interaction and Polarization Effect

In this section, the interaction of PS with the embedded 8HQ molecules is considered. It is evident that ionization potentials and electron affinities can be affected by the presence of a solvent, even with a small dielectric constant, due to the dipolar nature of 8HQ molecules and because charged molecules are involved in these quantities. The problem has been faced at two different levels of theory:

(1) by modeling the whole system as a periodic crystal (8HQ molecules embedded in PS) by means of a fully quantum mechanical description (DFT);

(2) by a hybrid description, namely a single 8HQ molecule in a polarizable continuum model (PCM). The aim is to establish whether the second theoretical model, much less time-expensive and computing-demanding, would represent a reasonable approach for the purposes of the present work.

For what concerns the first approach, we considered the explicit contribution of the surrounding PS to the relative stability of 8HQ tautomers by adopting a crystalline model of syndiotactic polystyrene (s-PS).[48] The complex polymorphic behavior of s-PS and its property to cocrystallize with a large variety of molecules to form host−guest molecular complexes have been extensively studied.[49,50] Depending on the size of the molecular guest, different kinds of hosting cavities can be formed to embed moieties. Small size molecules (including toluene) tend to be imprisoned as guests into cavities producing only minor changes to the packing of the polymer helices. Such complexes have been defined clathrate phases and are generally characterized by a guest/monomeric-unit molar ratio 1/4, with the exception of very tiny molecules (such as I_2 or CS_2) which can lead to multiple occupations of the same cavity. When the guest molecules are larger, like, e.g. 1,4-dimethyl-naphthalene or norbornadiene, another kind of complex can be established, defined as the intercalate phase. The guest molecules are not isolated into host cavities but contiguous inside layers intercalated with monolayers of enantiomorphous polymer helices. In this case, the guest/monomer-unit molar ratio is 1/2. The 8HQ molecules in the memory device polymeric film are in a guest/monomer-unit molar ratio of ∼1/4 (27%) with PS.[6] Due to the underlying synthetic technique, the 8HQ/PS mixture should be in an amorphous phase where 8HQ molecules are randomly spread into the bulk, but it could probably maintain the same crystalline complexation structure in the closest proximity of guest molecules, due to the large sizes of the polymer chains. On the other side, the DT-capped gold nanoparticles should not affect (upset) the local crystalline structures, having sizes much larger than the lattice cell. So, it is likely that a mixture of clathrate/intercalate phases coexists in the amorphous phase, depending on the local concentration of 8HQ molecules. We have considered both phases, the intercalate phase, where 8HQ molecules are in the most packed configuration (8HQ/PS-monomer-unit molar ratio of 1/2) and where dipole−dipole interactions between them could play a role and the clathrate phase (8HQ/PS-monomer-unit molar ratio of 1/4).

As an initial guess, we adopted the crystalline model (intercalate phase) established by X-ray diffraction measurements for 1,4-dimethyl-naphthalene in s-PS in the $P2_1/a$ space group.[48] This crystal lattice is composed by s-PS helicoidal chains along the [010] axis which are faced along the [100] axis (see Figure 2). The s-PS chains form bidimensional layers parallel to the (001) plane where in between 8HQ layers can be easily accommodated (Figure 3a). This structure was first fully optimized by molecular mechanics (CVFF force field[29−31]) which provided the cell constants $a = 17.110$, $b = 7.975$, $c = 16.463$, and $\beta = 121.3$ and then refined in the internal coordinates via periodic DFT calculations with the hybrid functional B3LYP and 6-31G* basis set (structure available in the Supporting Information file 1.cif). Because of the smaller steric encumbrance of 8HQ molecules, geometry optimizations caused a slight contraction of the original primitive lattice cell,[48] especially along the [001] axis. This is in agreement with results of Guerra et al. when changing guest molecules from 1,3,5-trimethyl-benzene to 1,4-dimethyl-naphthalene.[48] Then, one of the four enolic 8HQ molecules in the unit cell was substituted by a ketonic 8HQ (see Figure 2b). This new structure has been optimized in the $P1$ space group (structure in the Supporting Information file 2.cif). So, we found that the first "all-enolic" structure is more stable than the second "one-ketonic" structure with an energy difference of 0.37 eV. We remind here that for the isolated molecule we found the enolic form is more stable by 0.66 eV

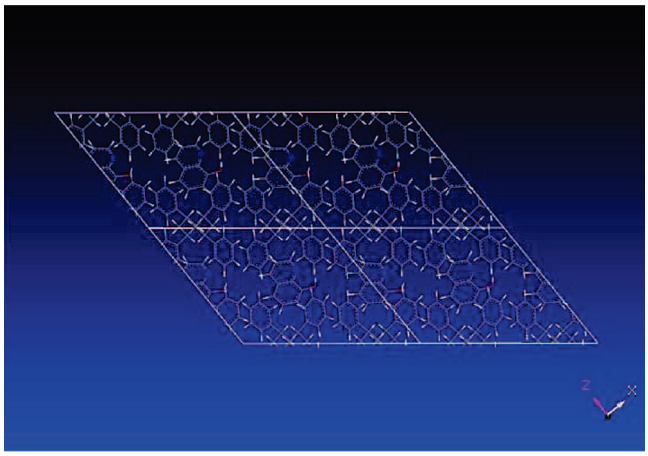

Figure 4. Crystalline model of s-PS clathrate with 8HQ moieties where the minimum distance between two 8HQ molecules is 7.9 Å.

than its ketonic tautomer at the same level of theory (see first row of Table 1). So, the global embedding effect of the crystalline structure on the single molecular tautomer stabilization accounts for 0.29 eV. It remains to establish the relative weight in the effect of intermolecular interactions between 8HQ molecules.

By substituting three of the four 8HQ molecules in the unit cell with naphthalene molecules (see Figure 2c), which approximately have the same encumbrance of 8HQ but vanishing permanent dipole moment, we obtained new optimized structures (Supporting Information files 3.cif and 4.cif) with a keto−enol energy difference of 0.34 eV. This means that the dipole−dipole interactions between 8HQ molecules tune the tautomeric equilibrium for 0.03 eV.

The clathrate phase has been also considered by eliminating two of the four 8HQ molecules in the unit cell: the initial guess of the clathrate unit cell has been obtained by considering the two 8HQ molecules corresponding to numbers 1 and 3 in Figure 3. The resulting crystal has been optimized according to the same computational scheme used for the intercalate phase (MM + DFT), but in the P1 space group, providing the cell constants $a = 17.368$, $b = 7.903$, $c = 14.691$, $\alpha = 81.4$, $\beta = 128.7$, and $\gamma = 90.3$ (see Figure 4; structures in Supporting Information files 5.cif and 6.cif). We obtained a further contracted unit cell with respect to the initial guess and a keto−enol energy difference of 0.47 eV, which is higher than that in the intercalate phase (0.37 eV), as we could expect because the clathrate phase is less dense and it must tend toward the vacuum conditions (0.66 eV).

Next, we studied the 8HQ-PS system by means of PCM,[16−20] by modeling the PS as a nonstandard toluene solvent with a dielectric constant $\varepsilon = 2.6$, which is the experimental value for the syndiotactic polystyrene. Within the PCM, the use of a toluene instead of a PS solvent reflects only on the so-called nonelectrostatic terms, such as the cavitation energy, the repulsion energy, and the dispersion energy, which do not change for small nuclear modifications of the solute molecule.[16] Hence, because we are interested in energy differences between solute molecules with very similar geometrical structures, the nonelectrostatic terms will almost cancel each other whatever the chemical nature of the solvent we are considering. On the contrary, the dielectric constant value to be used is a crucial parameter in determining the electrostatic solute−solvent interactions and so the solvation energies. By using the same B3LYP hybrid functional, as in the periodic calculations, with the N07D basis set, we found a keto−enol energy difference

TABLE 3: Solvation Energies of Neutral, Negative, and Positive 8HQ Tautomers (I and II) and Transition States (TSs) in PS (PCM Simulation, DFT with M052X Functional, and N07D Basis Set), and Tautomerization Energies and Barriers of Solvated 8HQ[a]

charge	$G_{I_{PS}} - G_I$	$G_{II_{PS}} - G_{II}$	$G_{TS_{PS}} - G_{TS}$	$G_{I_{PS}} - G_{II_{PS}}$	$\Delta G^{\ddagger}_{(I\rightarrow II)_{PS}}$
0	−8.4	−34.2	−23.0	−51.4	67.8
−1	−122.0	−137.5	−124.6	17.4	30.1
1	−144.2	−154.0	−144.5	33.1	32.2

[a] Energies are expressed in kilojoules per mole, and they all include the zero-point-energy corrections in the harmonic approximation.

TABLE 4: PS-Induced Polarization Energies on Neutral, Negative, and Positive 8HQ Tautomers I and II (E_{pol}), 8HQ−PS Interaction Energies (E_{int}), 8HQ Dipole Moments in PS (μ_{PS}), and in Vacuum (μ_{vac})[a]

	I	II	I^-	II^-	I^+	II^+
E_{pol}	1.5	9.9	4.2	8.9	1.5	4.9
E_{int}	−18.5	−53.8	−135.5	−157.1	−152.1	−170.3
μ_{PS}	3.71	8.94	2.36	6.40	2.96	6.14
μ_{vac}	2.99	6.63	1.67	4.69	2.55	4.93

[a] Energies are in kilojoules per mole, and dipole moments are in Debye.

of 0.39 eV, in good agreement with results obtained from periodic calculations. Indeed, this result is intermediate between the most packed crystalline structure (the intercalate phase), and the least dense one (the clathrate phase) we have considered.

Hence, we can not only assume that the interactions between neighbor 8HQ molecules have a negligible weight on the global solvation and polarization effect exerted by PS on the tautomeric equilibrium, but the isotropic continuum solvation model at the heart of the PCM approach is also a good approximation for the same purposes. In fact, the comparison between different crystalline periodic calculations and PCM witnesses the marginal influence of the different local nuclear arrangements of the solvent, crystalline or amorphous, on the tautomers stabilization. Indeed, the experimental procedure used to synthesize the most likely amorphous polymeric film, suggests an isotropic solvation model to be more realistic than a crystalline one. So, we decided to adopt the PCM for the following calculations, with the M052X functional previously tested for the isolated molecule to improve accuracy on relative energies.

In Table 3, we show the solvation energies obtained for the neutral, negative, and positive 8HQ molecule in its enolic and ketonic forms and transition states. The Gibbs free energies reported in Table 3 include the entropic, thermal, and zero-point energy corrections in the harmonic approximation for a temperature $T = 298.15$ K. The tautomerization energy, $G_{I_{PS}} - G_{II_{PS}}$, and the tautomerization barrier, $\Delta G^{\ddagger}_{(I\rightarrow II)_{PS}}$, of the neutral 8HQ in PS decreases with respect to the vacuum, although the keto tautomers do not reach a statistically relevant concentration: the Boltzmann enol−keton population ratio at the equilibrium is 1.0×10^9 at $T = 298.15$ K.

The PCM allows us to give a deeper insight on the solvent effect through a detailed analysis of the different contributions to the solvation. In the first row of Table 4, we show the polarization energy E_{pol}, which is defined as the difference between the energy of 8HQ calculated in vacuum and the same quantity evaluated using the electronic density perturbed by PS.[16] In Table 4, we also report the interaction energy E_{int}, namely the solute−solvent electrostatic interaction and the 8HQ dipole moments in vacuum and in PS. Whatever the net charge, the

TABLE 5: Electron and Hole Injection Barriers between 8HQ and the Aluminum Electrodes in Terms of Gibbs Free Energies (ϕ_e and ϕ_h, Respectively) in Vacuum and in PS[a]

	ϕ_e	ϕ_h
Al/8HQ (vacuum)	3.92	3.35
Al/8HQ (PS)	2.59	1.85
Au-DT/8HQ (PS)	≥2.0	≤2.4

[a] Energies in electronvolts.

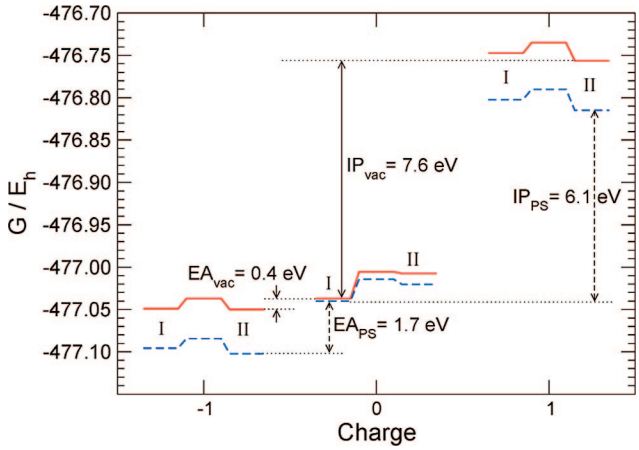

Figure 5. Energetic scheme of 8HQ equilibrium structures (I and II) and their tautomerization barriers as calculated in vacuum (straight lines) and in PS (dashed lines).

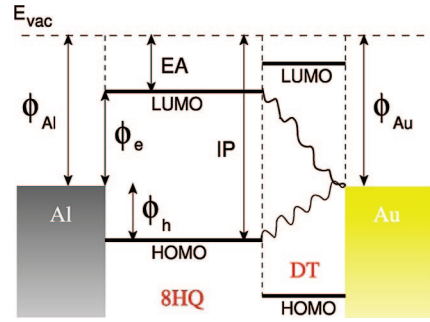

Figure 6. Qualitative scheme of the electron injection barrier ϕ_e and the hole injection barrier ϕ_h at the interfaces between 8HQ−Al and 8HQ−AuNPs.

TABLE 6: Electron Affinities and Ionization Potentials in Terms of Gibbs Free Energies of 8HQ in Vacuum, in PS, and under Different Electric Field Effects ($E_1 = 5.1 \times 10^7$ V/m, $E_2 = 2E_1$, and $E_3 = 20E_1$)[a]

environment	EA	IP
vacuum	0.36	7.63
PS	1.69	6.13
PS + E_1	1.70	6.11
PS + E_2	1.70	6.11
PS + E_3	1.75	6.07

[a] All results are from DFT (M052X) calculations. Energies are in electronvolts.

molecular polarizability and the dipole moment of the 8HQ keto forms are generally higher than those of the enolic counterparts and these properties impact on the stronger solvent-induced stabilization of the neutral keton (see Table 4). On the other hand, the solute−solvent interaction term prevails when the charged 8HQ are considered. As a consequence, the electron affinity of the PS-solvated 8HQ results to be remarkably higher and the ionization potential lower than those of the isolated molecule (see Table 6 and Figure 5).

5. Electron and Hole Injection Barriers

In this section, we make a further step within a bottom-up approach, from the study of the single-component microscopic features toward the explanation of the memory device macroscopic behavior. The first characteristic, the so-called bistability, which allows the apparatus to be used as a memory device and to classify it under the FET (field-effect-transistor) family, is the ability to switch from a low-conductivity state to a high-conductivity one by the application of low bias at the aluminum electrodes. The second feature is a large hysteresis width in the current−voltage plot, which implies a sharp-cut electric current difference between the two conductivity regimes when a specific voltage is applied. This characteristic permits to obtain a good accuracy and reliability on reading the boolean information about the conductivity state. In this way, it is possible to exploit the device as a write-read-erase memory, as long as three specific voltages can be chosen in order to write (switch on), read, and erase (switch off) the information (current flow). The third requirement is the qualitative and quantitative stability of the device properties under thousands of switching iterations (write-read-erase cycles).

Indeed, under the application of at least 2.8 V for less than 25 ns, the current intensity flowing through the memory device increases from 10^{-11} to 10^{-6} A, whereas at positive voltages lower than 2.8 V, the device remains in its conductivity regime, either high or low.[6] The application of an inverse bias of at least −1.8 V is required to make it switch back to its high-resistance regime. Our aim is a basic understanding of the molecular mechanisms which determine this particular field-effect behavior. The first requirement for the electric current to flow through the device is electron or hole injection from metal electrodes to the polymeric film.[51] It has been assessed from experimental evidence that the mean conductive molecular component is represented by the 8HQ molecules which determine the voltage thresholds at the aluminum interfaces,[4,6] but the hysteresis width and the I−V asymmetric behavior are caused by the presence of AuNPs and are sensitive to their concentration and size. On the contrary, the role played by the PS matrix is not evident in view of its substantial inertia. In the previous section we established how the PS matrix modifies the IP and EA of 8HQ. In a simple electron donor−acceptor model, where a 8HQ molecule in the PS environment and the metal electrode represent the redox couple, we can calculate the electron and hole injection barriers which are the Gibbs free energies required to transfer an electron from the aluminum electrode to an 8HQ molecule and viceversa, on the sole basis of thermodynamics (see Figure 6). This means that we neglect possible kinetic barriers present at the metal−molecule interface, and we only acknowledge the minimum energy required for the electron transfers when tunneling effects are negligible.

Considering the experimental aluminum work function $\phi_{Al} = 4.28$ eV,[52] we show in Table 5 the electron and hole injection barriers, ϕ_e and ϕ_h, respectively, as resulting from 8HQ IP and EA in vacuum and in PS:

$$\phi_e = \phi_{Al} - EA \quad (1)$$

$$\phi_h = IP - \phi_{Al} \quad (2)$$

The relevant role played by the PS matrix in lowering both the electron and the hole injection barriers is now evident. On the other side, the application of a bias to the aluminum electrodes produces an electric field through the polymeric film which

could affect the electronic properties of the dipolar 8HQ molecules. If we assume that the applied voltage to the aluminum electrodes does not spawn an electrostatic double-layer at the interface with the polymeric film, under the application of a bias of 2.8 V (the experimental threshold voltage to switch the device on), an average electric field of $E = 5.6 \times 10^7$ V/m would result through an isotropic dielectric 50 nm thick. By applying electric field perturbations corresponding to about E, $2E$, and $20E$, along the direction of the 8HQ dipole moments in PS (modeled with the same PCM), the 8HQ IP and EA change by just 55 meV (see Table 6). The last results represent the maximum interactions which could occur between the 8HQ molecules and the electric fields, because we have intentionally aligned the molecular dipole moments favorably with the electric fields. The electric field contribution can hence be considered negligible with respect to the solvation effect, for applied bias up to 20 times the threshold voltage.

The fact that $\phi_h < \phi_e$ should prove a hole transport mechanism, and the estimated ϕ_h value is in good agreement with the experimental threshold voltage of 2.8 V: indeed, if the asymmetry parameter was $\eta = 0.5$,[53−55] a voltage of 2.8 V between the aluminum electrodes would provide an injection energy of about η eV = 1.4 eV, close to $\phi_h = 1.85$ eV. It is worth noting that the barriers could be also lower than the calculated ones because the AuNPs increase the dielectric constant of the polymeric film. Indeed, ceteris paribus, when another kind of electron acceptor in the memory device is used, i.e. fullerenes instead of AuNPs,[4] the switching threshold does not change.

On the other hand, the asymmetry of the I−V plot[3] does not exclude the possibility of η values different from 0.5, which could turn out from a different electric response of the two polymeric film−electrode interfaces to the applied voltage: for instance, the positive voltage applied in the write phase, could induce an 8HQ dipolar orientation at the aluminum interfaces which could persist even at low negative voltages (erase phase). In fact, the $8HQ^+$ molecules, generated in the hypothesis of a hole transport mechanism, would be in their strongly dipolar II^+ form which easily aligns with the electric field (see Table 4). In this case, it is not trivial to establish which conduction mechanism is active without an explicit study of the aluminum-film interfaces. Furthermore, the possible occurrence of periodic molecular adsorptions on the metal surfaces, such as 8HQ monolayers, would change the aluminum work functions and hence the resulting injection barriers (see eqs 1 and 2).

It is even more difficult to assess the accurate injection barriers at the 8HQ−AuNP interface. Actually, the work function of bare gold surfaces is 5.1 eV,[52,55] but it lowers with decreasing thickness of gold films (a 20 nm thick film shows $\phi_{Au} = 4.9$ eV[56]), and it is known that alkanethiols capping decreases the metal work function causing an increase in the hole injection barrier[56] ($\phi_{Au} = 4.1$ eV for exadecanethiol-capped 20 nm gold films[56]). Furthermore, with decreasing sizes of spherical-like gold nanoparticles, quantum size effects become evident in Coulomb staircase-capacitance behavior.[57] So, if we assume that the AuNPs work functions are $\phi_{Au} \leq 4.1$ eV, the resulting barriers at the 8HQ interface will be $\phi_e^{Au} \geq 2.0$ and $\phi_h^{Au} \leq 2.4$. This certainly means that the electron transfer between the AuNPs and 8HQ is not allowed at low bias. However, it remains to assess if the electric field along with the dodecanethiols monolayer effects could vary the AuNPs barriers,[58,59] given that the IPs and EAs of solvated 8HQ do not show substantial changes under the application of electric fields.

6. Conclusions

We studied the keto−enolic tautomerization of the neutral, negative, and positive 8-hydroxyquinoline molecule in vacuum and in polystyrene by means of DFT and coupled cluster methods in order to obtain information on the microscopic mechanisms tuning the behavior of a polymer based memory device. We found that in both environments the neutral molecule is more stable in its enolic form, whereas the keto form is preferred when the molecule is positively or negatively charged. The energy differences and the kinetic barriers between tautomers result to be much larger than the thermal energy at room temperature. In general, the ketonic forms have larger dipole moments than the enolic ones. The polystyrene solvation effect on the neutral molecule tautomerization was taken into account by means of periodic calculations of a crystalline structure which were found to be in agreement with PCM calculations. The calculated molecular ionization potential and electron affinity result to be significantly decreased and increased respectively by the polystyrene solvation effect. We hence calculated the electron and hole injection barriers at the molecule/aluminum electrode interface as resulting from the difference between the aluminum work function and the polystyrene-solvated 8-hydroxyquinoline electron affinity and ionization potential respectively, which confirm a low-conductivity state of the device at zero bias. The application of low and high electric fields on the solvated molecule was found to be almost ineffective on the molecular properties. Assuming a symmetric electric response at the two aluminum electrodes, the experimental required voltage to switch the device to a high-conductivity state could, according to our calculations, provide the hole injection energy, giving clues for a hole transport mechanism. However, a deeper and explicit study of the electrodes/polymeric film interfaces is required in order to provide further detailed information. Work along these and related lines is presently being undertaken in our laboratory.

Acknowledgment. The work was funded from the PON 1575/2004 Project High Performance Cooperative Distributed System for Multidisciplinar Scientific Elaborations (S.Co.P.E. project from the Italian initials) and by MIUR (PO.DI.ME project). Dr. Michele Pavone and Dr. Malgorzata Biczysko are kindly acknowledged for fruitful scientific discussions. The VILLAGE network (http://village.unina.it) and CINECA are acknowledged for their computational facilities.

Supporting Information Available: Additional information as noted in text. This material is available free of charge via the Internet at http://pubs.acs.org.

References and Notes

(1) Scott, J. *Science* **2004**, *304*, 62.
(2) Chen, Y.; Jung, G.-Y.; Ohlberg, D.; Li, X.; Stewart, D.; Jeppesen, J.; Nielsen, K.; Stoddart, J.; Williams, R. *Nanotechnology* **2003**, *14*, 462.
(3) Yang, Y.; Ouyang, J.; Ma, L.; Tseng, R.-H.; Chu, C.-W. *Adv. Funct. Mater.* **2006**, *16*, 1001.
(4) Paul, S. *IEEE Trans. Nanotechnol.* **2007**, *6*, 191.
(5) Muccini, M. *Nat. Mater.* **2006**, *5*, 605.
(6) Ouyang, J.; Chu, C.-W.; Szmanda, C.; Ma, L.; Yang, Y. *Nat. Mater.* **2004**, *3*, 918.
(7) Kwok, K.; Ellenbogen, J. *Mater. Today* **2002**, 28.
(8) Singh, J. *Smart Electronic Materials*; Cambridge University Press: New York, 2005.
(9) Goodisman, J. *Electrochemistry: Theoretical Foundations*; Wiley-Interscience: New York, 1987).
(10) Schmickler, W. *Interfacial Electrochemistry*; Oxford University Press: New York, 1996.
(11) Frisch, M. J.; Trucks, G. W.; Schlegel, H. B.; Scuseria, G. E.; Robb, M. A.; Cheeseman, J. R.; Montgomery, J. A., Jr.; Vreven, T.; Kudin, K. N.;

Burant, J. C.; *Gaussian development version*; revision G.01, Gaussian, Inc.: Wallingford, CT, 2006.

(12) Becke, D. *J. Chem. Phys.* **1993**, *98*, 5648.

(13) Zhao, Y.; Schultz, N.; Truhlar, D. *J. Chem. Theory Comput.* **2006a**, *2*, 364.

(14) Zhao, Y.; Truhlar, D. *Acc. Chem. Res.* **2007**, *41*, 157.

(15) Barone, V. unpublished.

(16) Tomasi, J.; Mennucci, B.; Cammi, R. *Chem. Rev.* **2005**, *105*, 2999.

(17) Cossi, M.; Scalmani, G.; Rega, N.; Barone, V. *J. Chem. Phys.* **2002**, *117*, 43.

(18) Scalmani, G.; Frish, M. J.; Mennucci, B.; Tomasi, J.; Cammi, R.; Barone, V. *J. Chem. Phys.* **2006**, *124*, 094107.

(19) Improta, R.; Scalmani, G.; Frisch, M.; Barone, V. *J. Chem. Phys.* **2007**, *127*, 074504.

(20) Improta, R.; Barone, V.; Scalmani, G.; Frisch, M. *J. Chem. Phys.* **2006**, *125*, 054103.

(21) Frisch, M. J.; Trucks, G. W.; Schlegel, H. B.; Scuseria, G. E.; Robb, M. A.; Cheeseman, J. R.; Montgomery, J. A., Jr.; Vreven, T.; Kudin, K. N.; Burant, J. C.; *Gaussian 03*; revision C.02, Gaussian, Inc.: Wallingford, CT, 2004.

(22) Barone, V.; Cimino, P.; Stendardo, E. *J. Chem. Theory Comput.* **2008**, *4*, 751.

(23) Ayala, P. Y.; Schlegel, H. B. *J. Chem. Phys.* **1997**, *107*, 375.

(24) Knowles, P. J.; Hampel, C.; Werner, H.-J. *J. Chem. Phys.* **1993**, *99*, 5219.

(25) Szabo, A.; Ostlund, N. S. *Modern Quantum Chemistry*; Dover Publications Inc.: Mineola, NY, 1996.

(26) Werner, H.-J.; Knowles, P. J.; Lindh, R.; Manby, F. R.; Schütz, M.; Celani, P.; Korona, T.; Rauhut, G.; Amos, R. D.; Bernhardsson, A.; Molpro; version 2006.1, 2006.

(27) Dunning, T. H., Jr. *J. Chem. Phys.* **1989**, *90*, 1007.

(28) http://accelrys.com (accessed Oct 2008).

(29) Hardy, B. J.; Sarko, A. *J. Comput. Chem.* **1993**, *7*, 831.

(30) Hagler, A. T.; Lifson, S.; Dauber, P. *J. Am. Chem. Soc.* **1979**, *101*, 5122.

(31) Siebert, H. C.; Reuter, G.; von der Lieth, R. S. C. W.; Dabrowski, J. *Biochemistry* **1992**, *31*, 6962.

(32) Saunders, V. R.; R. Dovesi, R. C.; Causà, M.; Harrison, N. M.; Zicovich-Wilson, C. M. *CRYSTAL '98 User Manual*; Turin University: Turin, Italy, 1999.

(33) Dovesi, R.; Saunders, V. R.; Orlando, R.; Zicovich-Wilson, C. M.; Pascale, F.; Civalleri, B.; Doll, K.; Bush, I. J.; D'Arco, P.; Lunell, M. *Crystal 2006 User Manual*; Turin University: Turin, Italy, 2007.

(34) Dovesi, R.; Pisani, C.; Roetti, C.; Saunders, V. R. *Phys. Rev. B* **1983**, *28*, 5781.

(35) Causà, M.; Dovesi, R.; Orlando, R.; Pisani, C.; Saunders, V. R. *J. Phys. Chem.* **1988**, *92*, 909.

(36) Pisani, C.; Dovesi, R.; Roetti, C. *Lecture Notes in Chemistry*; Springer-Verlag: Heidelberg, Germany, 1988.

(37) Zicovich-Wilson, C. M.; Dovesi, R. *Int. J. Quantum Chem.* **1998**, *67*, 299.

(38) Doll, K.; Harrison, N. M.; Saunders, V. R. *Int. J. Quantum Chem.* **2001**, *82*, 1.

(39) Doll, K. *Comput. Phys. Commun.* **2001**, *137*, 74.

(40) Civalleri, B.; D'Arco, P.; Orlando, R.; Saunders, V. R.; Dovesi, R. *Chem. Phys. Lett.* **2001**, *348*, 131.

(41) Ditchfield, R.; Hehre, W. J.; Pople, J. A. *J. Chem. Phys.* **1971**, *54*, 274.

(42) Mason, S. F. *J. Chem. Soc.* **1957**, 4874.

(43) Roychowdhury, P. *Acta Cryst. B* **1978**, *34*, 1047.

(44) Banerjee, T.; Saha, N. *Acta Cryst. C* **1986**, *42*, 1408.

(45) Bardez, E.; Devol, I.; Larrey, B.; Valeur, B. *J. Phys. Chem. B* **1997**, *101*, 7786.

(46) Shchavlev, A.; Pankratov, A.; Shalabay, A. *Int. J. Quantum Chem.* **2005**, *106*, 876.

(47) Zhao, J.-Y.; Zhou, Z.-Y.; Su, Z.-M.; Xie, Y.-Z.; Sun, G.-Y.; Wu, X. *Can. J. Chem.* **2006**, *24*, 724.

(48) Tarallo, O.; Petraccone, V.; Venditto, V.; Guerra, G. *Polymer* **2006**, *47*, 2402.

(49) Guerra, G.; Vitagliano, M.; Rosa, C. D.; Petraccone, V.; Corradini, P. *Macromolecules* **1990**, *23*, 1539.

(50) Chatani, Y.; Stimane, Y.; Inoue, Y.; Inagaki, T.; Ishioka, T.; Iijtsu, T.; Yukimori, T. *Polymer* **1992**, *33*, 488.

(51) Zaumseil, J.; Sirringhaus, H. *Chem. Rev.* **2007**, *107*, 1296.

(52) Eastment, R. M.; Mee, C. H. B. *J. Phys. F* **1973**, *3*, 1738.

(53) Tian, W.; Datta, S.; Hong, S.; Reifenberger, R.; Henderson, J. I.; Kubiak, C. P. *J. Chem. Phys.* **1998**, *109*, 2874.

(54) Adams, D. M.; Brus, L.; Chidsey, C. E. D.; Creager, S.; Creutz, C.; Kagan, C. R.; Kamat, P. V.; Lieberman, M.; Lindsay, S.; Marcus, R. A.; et al. *J. Phys. Chem. B* **2003**, *107*, 6668.

(55) Engelkes, V. B.; Beebe, J. M.; Frisbie, C. D. *J. Am. Chem. Soc.* **2004**, *126*, 14287.

(56) de Boer, B.; Hadipour, A.; Mandoc, M. M.; van Woudenbergh, T.; Blom, P. W. M. *Adv. Mater.* **2005**, *17*, 621.

(57) Han, M. Y.; Zhou, L.; Quek, C. H.; Li, S. F. Y.; Huang, W. *Chem. Phys. Lett.* **1998**, *287*, 47.

(58) Heimel, G.; Romaner, L.; Brédas, J.-L.; Zojer, E. *Surf. Sci.* **2006**, *600*, 4548.

(59) Crispin, X.; Geskin, V. M.; Bureau, C.; Lazzaroni, R.; Schmickler, W.; Brédas, J.-L. *J. Chem. Phys.* **2001**, *115*, 10493.

JP804274R